First Experimental Constraint on the ^{59}Fe$(n,\gamma)^{60}$Fe Reaction Cross Section at Astrophysical Energies via the Coulomb Dissociation of ^{60}Fe

E. Uberseder,[1,*] T. Adachi,[2] T. Aumann,[3,4] S. Beceiro-Novo,[5] K. Boretzky,[4] C. Caesar,[3] I. Dillmann,[4] O. Ershova,[6] A. Estrade,[4,7] F. Farinon,[4] J. Hagdahl,[8] T. Heftrich,[6] M. Heil,[4] M. Heine,[3] M. Holl,[3] A. Ignatov,[3] H. T. Johansson,[8] N. Kalantar,[2] C. Langer,[6] T. Le Bleis,[9] Yu. A. Litvinov,[4] J. Marganiec,[10] A. Movsesyan,[3] M. A. Najafi,[2] T. Nilsson,[8] C. Nociforo,[4] V. Panin,[3] S. Pietri,[4] R. Plag,[6] A. Prochazka,[4] G. Rastrepina,[4] R. Reifarth,[6] V. Ricciardi,[4] C. Rigollet,[2] D. M. Rossi,[4,†] D. Savran,[10,11] H. Simon,[4] K. Sonnabend,[6] B. Streicher,[2] S. Terashima,[4] R. Thies,[8] Y. Togano,[12] V. Volkov,[3] F. Wamers,[3,4] H. Weick,[4] M. Weigand,[6] M. Wiescher,[1] C. Wimmer,[6] N. Winckler,[4] and P. J. Woods[13]

[1]*Department of Physics, University of Notre Dame, Notre Dame, Indiana 46556, USA*
[2]*KVI, University of Groningen, Zernikelaan 25, NL-9747 AA Groningen, The Netherlands*
[3]*Institut für Kernphysik, Technische Universität Darmstadt, 64289 Darmstadt, Germany*
[4]*GSI Helmholtzzentrum für Schwerionenforschung GmbH, D-64291 Darmstadt, Germany*
[5]*Departamento de Física de Partículas, Universidade de Santiago de Compostela, 15706 Santiago de Compostela, Spain*
[6]*Goethe-Universität Frankfurt am Main, 60438 Frankfurt am Main, Germany*
[7]*Department of Astronomy and Physics, Saint Mary's University, Halifax B3H3C3, Canada*
[8]*Fundamental Fysik, Chalmers Tekniska Högskola, S-412 96 Göteborg, Sweden*
[9]*Physik Department E12, Technische Universität München, 85748 Garching, Germany*
[10]*ExtreMe Matter Institute EMMI, GSI Helmholtzzentrum für Schwerionenforschung GmbH, D-64291 Darmstadt, Germany*
[11]*Frankfurt Institute for Advanced Studies FIAS, D-60438 Frankfurt, Germany*
[12]*RIKEN Nishina Center, Saitama 351-0198, Japan*
[13]*School of Physics and Astronomy, University of Edinburgh, Edinburgh EH9 3JZ, United Kingdom*

(Received 8 November 2013; revised manuscript received 4 February 2014; published 28 May 2014)

The radionuclide ^{60}Fe has been of great interest to the nuclear astrophysics community for over a decade. An initial discrepancy between the observed and modeled Galactic ^{60}Fe/^{26}Al ratio motivated numerous studies focused on the nucleosynthesis of these two isotopes, though the cross section of the primary astrophysical production reaction, ^{59}Fe$(n,\gamma)^{60}$Fe, has remained purely theoretical. The present work offers a first experimental constraint on the ^{59}Fe$(n,\gamma)^{60}$Fe cross section at astrophysical energies, obtained indirectly via Coulomb dissociation, and demonstrates that the theoretical reaction rates used in present stellar models are not highly erroneous.

DOI: 10.1103/PhysRevLett.112.211101 PACS numbers: 26.20.Np, 25.70.De, 95.85.Pw

The interest of the nuclear astrophysics community in the long-lived radionuclide ^{60}Fe began with the observation of the decay signatures of ^{26}Al [1]. These observations provided definitive evidence of active nucleosynthesis in the Galaxy [2], though the stellar origins of the isotope were unknown. Many candidate sites were proposed for ^{26}Al nucleosynthesis, including asymptotic giant branch stars, novae, Wolf-Rayet (W-R) stars, and type-II supernovae (SN-II). Strong observational constraints on ^{26}Al production sites were first given by the COMPTEL γ-ray telescope aboard the orbiting Compton Gamma Ray Observatory, which provided a Galactic map of ^{26}Al radioactivity with good resolution. The inhomogeneous distribution of ^{26}Al, and the excellent overlap of the ^{26}Al sky map with observations of bremsstrahlung radiation resulting from free electrons scattering off of ionized gas, argued strongly for massive star production of ^{26}Al [3,4].

Studies then pivoted to determining which subclass of massive stars were primarily enriching the interstellar medium (ISM). Massive stars with $M/M_\odot < 35$ were expected to eject ^{26}Al only during the SN-II, while more massive stars were thought to enrich the ISM through winds during the W-R phases in addition to the final Type-Ibc supernovae. For a definitive determination, it was proposed to simultaneously observe the ratio of ^{60}Fe/^{26}Al. The isotope ^{60}Fe was predicted to be synthesized in similar stellar zones as ^{26}Al, with the exception of the main sequence contribution ejected via winds, and subsequently coenrich the ISM during the final supernova events. The contribution of ^{60}Fe from stars with $M/M_\odot > 35$ was initially expected to be small; therefore, if the ^{60}Fe/^{26}Al was well predicted by models of stars with $M/M_\odot < 35$, this would indicate that these objects were the primary producers of ^{26}Al [3,5]. Initial predictions of the ^{60}Fe/^{26}Al ratio gave 16% [6], though only an upper limit was available from the COMPTEL instrument.

A good observational constraint on the line flux ratio came from the INTEGRAL and RHESSI missions, the former giving a value of $16\% \pm 5\%$ [7] and the latter $14.8\% \pm 6\%$ [8,9]. These observational ratios were in good agreement with the initial model predictions for massive stars with $M/M_\odot < 35$, which would have implied that

these stars were the primary producers of Galactic ^{26}Al. In the intervening time between the first model prediction and the INTEGRAL and RHESSI observations, the stellar models had been updated, with all newer predictions trending significantly above the observational value [10,11]. It was subsequently argued that an additional contribution of ^{26}Al from W-R stars was required [12], and much effort was expended to resolve the discrepancy and examine the underlying uncertainties.

Inherent astrophysical uncertainties, including IMF slopes, mass loss rates, and convective conditions, still exist within the stellar models [13]. Additionally, a recent work has demonstrated that uncertainties in the helium burning reaction rates could strongly influence the modeled ^{26}Al and ^{60}Fe production in massive stars [14]. Regardless, all models are critically dependent on accurate knowledge of the production and destruction rates of the involved nuclei for meaningful and reliable predictions of the flux ratio. Interestingly, the first prediction of the ^{60}Fe/^{26}Al line flux ratio used values for the primary production and destruction cross sections of ^{60}Fe that differed from all subsequent predictions by approximately a factor of 2 in the direction of increasing ^{60}Fe yields [15]. As both the original and the newer recommended rates were fully theoretical, this discrepancy served as a motivation to experimentally constrain these crucial cross sections.

The isotope ^{60}Fe is produced in massive stars by a series of neutron captures on stable iron. The short lifetime of ^{59}Fe requires episodes of high neutron flux to bridge the instability, as is characteristic of late-stage convective shell burning in massive stars [13,16]. The primary destruction of ^{60}Fe in these objects occurs via an additional neutron capture. The first measurement of the destruction reaction $^{60}\mathrm{Fe}(n,\gamma)^{61}\mathrm{Fe}$ was performed by direct neutron activation on a ^{60}Fe target mined from a copper beam dump [17]. The short terrestrial half-life of ^{59}Fe (44.5 d [18]) prohibits a sufficiently large sample to be manufactured; therefore, a direct determination of the production cross section, $^{59}\mathrm{Fe}(n,\gamma)^{60}\mathrm{Fe}$, is difficult. The present work constrains this capture cross section using the time-reversed photodissociation reaction $^{60}\mathrm{Fe}(\gamma,n)^{59}\mathrm{Fe}$ studied via the Coulomb dissociation of a relativistic ^{60}Fe beam.

The experiment was performed at the GSI Helmholtzzentrum für Schwerionenforschung in Darmstadt, Germany. The primary ^{64}Ni beam was accelerated by the SIS18 synchrotron to an energy of 660 AMeV and impinged upon a 2.5 g/cm^2 Be production target. The ^{60}Fe projectile fragments were separated using the fragment separator FRS [19] and delivered to the R^{3}B-LAND setup in Cave C with rates of approximately 2.0–2.5×10^4 ions over spills lasting approximately 8 sec, energies of 540 AMeV, and a magnetic rigidity of $B\rho = 8.76$ Tm.

For the Coulomb dissociation measurement, a lead target with a thickness of 515 $\mathrm{mg/cm}^2$ was used. To quantify the nuclear dissociation component and the setup-induced background, runs were taken with a 558 $\mathrm{mg/cm}^2$ carbon target and an empty target frame, respectively. The identification of the incoming ion was performed using the rigidity setting of the separator, a velocity measurement over the 54.8 m flight path from the last focal plane of the FRS to Cave C, and the energy loss in a 300 μm thick silicon pin diode. Incoming ions were tracked onto the target using a pair of 300 μm thick double-sided silicon strip detectors (DSSDs) located 6.4 and 3.7 cm upstream of the target. Outgoing heavy fragments were tracked directly after the target using two additional DSSDs, placed 11.1 and 13.9 cm downstream from the target. Heavy fragments were diverted by approximately 15 deg using the ALADIN dipole magnet. The fragments were tracked downstream from the dipole magnet using two scintillating fiber detectors [20] located 4.69 and 6.13 m from the midpoint of ALADIN, and, after a flight path of approximately 11.5 m from the target, they impinged on two scintillating time-of-flight (TOF) walls. Neutrons from the reaction were measured using the LAND detector located 12.7 m downstream from the target on the beam axis. The absolute trigger efficiency for LAND is approximately 94% for neutrons of the present energy [21], and a detailed description of the detector can be found in Ref. [22]. Electromagnetic radiation emitted from the deexcitation of heavy fragments was detected using a 4π NaI calorimeter composed of 160 independent crystals surrounding the target [23]. The experimental setup allows for the complete reconstruction of the four-momenta of all incoming ions and outgoing reaction products, and therefore the excitation energy of the projectile before breakup. The energy resolution of the setup for this particular experiment varied from 0.5 MeV at the $1n$ neutron threshold, to 1.5 MeV at 25 MeV.

The excellent separation and therefore $B\rho$ discrimination provided by the FRS, in addition to accurate velocity and charge measurements of the incoming ion species, allowed for software selection of ^{60}Fe ions with a negligible background. An additional software cut imposed the condition that the energy loss in the TOF walls must correspond to $Z = 26$, thus restricting event acceptance to unreacted incoming beam and neutron-dissociated fragments. Requiring an additional trigger from the LAND detector reduces the accepted events primarily to those resulting from a neutron dissociation, with a small contamination arising from LAND triggers caused by secondary events in the TOF walls. The mass of the outgoing fragment was also reconstructed, and a further reduction in the background contamination was achieved by forcing consistency between the measured number of neutrons in the reaction and the outgoing iron fragment of a corresponding mass. A fragment mass resolution of $\sigma = 0.5\%$ was achieved in the present measurement.

The number of n-neutron events, where n is the number of detected neutrons, fulfilling the above requirements with

a reconstructed excitation energy E was normalized to the total number of counts triggering the TOF walls and falling within the charge cut for each target type. Such a scaling implicitly compensates for the efficiency of fragment detection as well as for differences in the number of total incoming ions. The nuclear dissociation component in the lead runs was determined from the carbon target data, where the carbon yields were rescaled to account for differences in target thickness and normalized by an additional factor α, which corrects for the variance in the nuclear dissociation cross sections of carbon and lead. In the present work, a value of α was adopted based on the black disk approximation. The chosen parameter could experimentally be verified by comparing the relative yields for the two targets in reaction channels where Coulomb dissociation is energetically unfavorable, such as high-multiplicity neutron emission, which is suppressed by the adiabatic cutoff in the virtual photon spectrum.

The Coulomb excitation cross section can be expressed in terms of the real-photon absorption cross section using the virtual-photon method [24], which may in turn be parametrized using γ-ray strength functions $f_{\lambda\pi}(E_\gamma)$ for a given multipolarity $\lambda\pi$. The normalized experimental yield in the n-neutron channel is then written in terms of these quantities as

$$Y_n(E) = (\pi\hbar c)^2 \sum_{m\lambda\pi} M_{m,n} \times \int dE' n_{\lambda\pi}(E') E'^{2\lambda-2} f_{\lambda\pi}(E') \times \sum_J \frac{(2J+1)}{(2I+1)} b_m(E', J) R_{mn}(E', E, J), \quad (1)$$

where $n_{\lambda\pi}(E')$ is the virtual photon number for a given multipolarity $\lambda\pi$, J is the spin-parity combination populated by the excitation of the ground state with spin I, and $M_{m,n}$ is the mass matrix representing the probability that an m-neutron event survives the fragment-mass cut on an n-neutron event. It should be noted that the neutron branching ratio b_m and response function $R_{mn}(E', E, J)$ both have a J dependence when angular momentum is considered in the excitation formalism.

The response function and neutron branching ratios were determined in the present work employing data generated from complex statistical model Monte Carlo (SMMC) simulations. The decay of excited ^{60}Fe in the energy range of 8.82–30 MeV over all populated J^π configurations was taken into account. Pre-equilibrium reactions were considered by assuming the initial state was in a $1p$–$1h$ configuration. Using the two-component exciton model, full cumulative distribution functions (CDFs) considering particle emission, particle-hole scattering, and pair transformation were formulated for each step towards equilibrium [25], with a random number dictating the subsequent configuration. If predefined conditions on exciton number were fulfilled, all following CDFs were generated using a standard equilibrium statistical decay formalism [26,27], and the iterations were repeated until all excitation energy had been liberated in particle or γ-ray emission. The results of the SMMC simulations were used to generate the branching ratios needed in Eq. (1). The SMMC simulated neutrons and γ rays were boosted into the reference frame of the average incoming projectile, and served as input for an R3BRoot [28] simulation of the experimental setup. The detector interactions generated using the latter were processed through routines replicating the signal processing of the acquisition electronics, and then given to the identical analysis routines used for the real data. This procedure yielded simulated experimental observables with known initial conditions, which could then be used to calculate the elements of the response matrix.

The $E1$ γ-ray strength function was convoluted as defined by Eq. (1), and then compared directly to the experimental yield. To account for deformation, the Lorentzian parametrization of Ref. [29] was utilized, where ^{60}Fe was treated as axially deformed with a value of $\beta = 0.211$ taken from theory [30]. The energy dependent width takes the form $\Gamma(E_\gamma) = \Gamma_0(E_\gamma/E_0)^\delta$, and values of δ of 0.0 [31], 0.5 [32], and 2.0 [33] were tested in the present work. A value of $\delta = 0.5$ was found to give the best agreement with the data while maintaining a reasonable $E1$ giant dipole resonance (EGDR) parametrization. The $E1$ strength functions were fitted to the data with three free parameters ($\sigma_{\pi\lambda}\Gamma_0$, Γ_0, and E_0) using log-likelihood and χ^2 minimization techniques, with both methods yielding consistent results. The $M1$ and $E2$ contributions to the excitation strength were considered, but left fixed in the fitting at parametrizations from systematics [34].

The raw lead-target dissociation distribution (black circles) before normalization and background subtraction can be seen in the upper frame of Fig. 1 as a function of reconstructed excitation energy, where the contributions from $1n$ and $2n$ dissociation have been summed. The background components from nuclear dissociations as measured with the carbon target (green) and the ambient dissociation background (blue) taken with the empty target frame are shown as shaded regions representing proportions of the total dissociation. These components have been scaled appropriately for number of incoming ions, target thickness, and differences in the nuclear interaction strength and their statistical uncertainties are represented by black lines. The fitted Coulomb dissociation contribution (red) reproduces well the difference between the summed measured background contributions and the total dissociation data. The shape of this dissociation distribution is heavily driven by the response function of the experimental setup, as well as the separation energies for $1n$ and $2n$ dissociation in ^{60}Fe, and the red region represents the electromagnetic dissociation contribution parametrized by the γ-ray strength function after the convolution given in Eq. (1). While the EGDR peak strength strongly

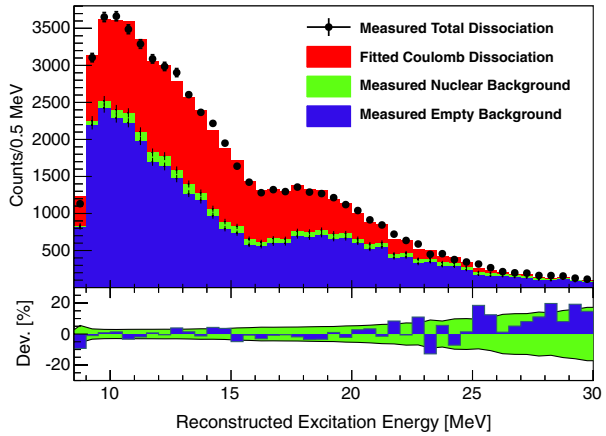

FIG. 1 (color online). Total measured dissociation of ^{60}Fe shown in comparison with the measured background components and the fitted Coulomb dissociation contribution. The lower panel shows the percent deviation of the fitted total dissociation from the measured spectrum. The shaded region represents the 1σ statistical uncertainty in the measured Coulomb dissociation distribution.

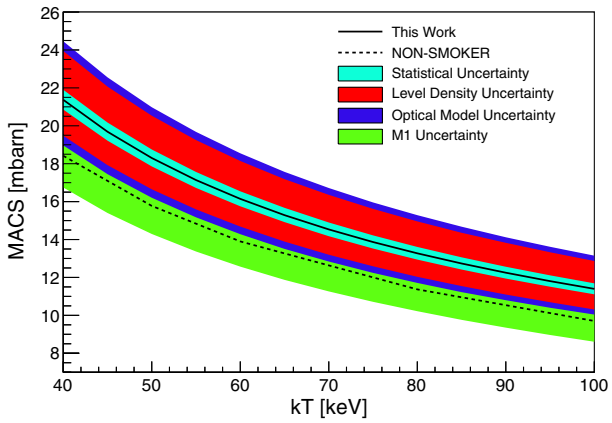

FIG. 2 (color online). Calculated MACS for $^{59}\mathrm{Fe}(n,\gamma)^{60}\mathrm{Fe}$. The shaded regions represent the predominant uncertainties of the method. The purely theoretical result of NON-SMOKER [37] is shown for comparison.

contributes to the structure at 18 MeV, it should be noted that the peak in reconstructed energy is enhanced by the valley at 16 MeV. This is due to the diminished acceptance of the LAND detector for high energy neutrons prior to the full opening of the $2n$ channel. The background spectrum has a similar peaking structure, as these are also real neutron dissociation events governed by the interplay of particle thresholds and detector acceptance. The bottom frame of Fig. 1 shows the percent deviation (blue) between the fitted Coulomb dissociation component added to the background and the total dissociation data. The shaded region (green) represents the combined 1σ statistical uncertainty from the total dissociation and background measurements. The EGDR parameters extracted from the fit were $\sigma_{E1}\Gamma_0 = 565(15)$ mb MeV (101% of the energy-weighted sum rule), $\Gamma_0 = 8.6(4)$ MeV, and $E_0 = 18.6(1)$ MeV. These extracted parameters correspond to those of a spherical nucleus of mass number 60, though the fitting routine splits the GDR into two resonance shapes using the deformation formalism described above. The large spreading width is interpreted as a consequence of the energy dependent damping of the GDR width [32,33] at low γ-ray energies; adopting a value of $\delta = 0$ reduces the fitted width by approximately 15% albeit with a significant increase in the reduced χ^2 statistic.

The γ-ray strength function is an important ingredient in the calculation of neutron capture in the Hauser-Feshbach theory, as it governs the photon-transmission term and therefore scales the cross section. If the γ-ray strength function can experimentally be determined, a major source of uncertainty in the theoretical rate determination would be removed. Such a technique has recently been successful in indirect determinations of neutron capture cross sections from total photoabsorption measurements [35,36].

Figure 2 shows a calculation of the Maxwellian averaged neutron capture cross section (MACS) of ^{59}Fe using the γ-ray strength function fitted to the Coulomb dissociation measurement. Also shown is the NON-SMOKER [37] cross section for comparison. The statistical uncertainty was determined from a Monte Carlo resampling of the data from the lead, carbon, and empty frame targets. Each trial data set was refit, resulting in a new γ-ray strength function parametrization. The major theoretical uncertainties in the method, coming from the optical model and the adopted level density, were also studied using Monte Carlo techniques. In the calculation of the cross sections, the equivalent square well [38,39] was used to determine the neutron transmission term. For the Monte Carlo analysis, the radius and diffuseness of the underlying diffuse edge potential were resampled from Gaussian distributions with the mean values fixed at their nominal values and 1σ parameters corresponding to 15% and 25% of the mean, respectively. The corresponding equivalent square well parameters were then recalculated as were the resulting neutron transmission terms for the particular Monte Carlo event. To treat the nuclear level densities with the Monte Carlo technique, experimental neutron s-wave level spacings from RIPL3 [40] were used to determine an experimental level density parameter a in the back-shifted Fermi gas model across the chart of nuclei. These experimental parameters were then compared to their theoretical equivalents [41] calculated at the neutron separation energy, and a distribution of the deviations was determined. This distribution was nearly Gaussian, with a 1σ width of approximately 4.8%, and was used to resample the level density parameter utilized in the Hauser-Feshbach calculation of the neutron capture cross section. In Fig. 2, each colored error band represents the increase in the deviation of the 15.9% and 84.1% quantiles from the median of the

MACS distribution due to the addition of the particular contribution into the Monte Carlo calculation. An additional source of uncertainty in the MACS determination arises from the $M1$ contribution. In the present work, the $M1$ strength was fixed from systematics. While contributing little to the Coulomb dissociation cross section, the $M1$ contribution to the neutron capture cross section can be significant. Recent studies have shown that the treatment of the $M1$ strength used presently may be unrealistic [42]. Furthermore, ^{59}Fe dissociation data were also taken during the measurement. The comparisons of the average p-wave radiative width from direct $^{58}\mathrm{Fe}(n,\gamma)^{59}\mathrm{Fe}$ studies [43,44] with those derived using the present method indicate the inclusion of the $M1$ contribution from systematics is too strong. Unfortunately, the present measurement offers little constraint on the $M1$ component. To compensate for this ambiguity in the uncertainty calculation, the data were refit with no $M1$ component, and the MACS recalculated. The deviation was added quadratically to the lower bound of the 1σ error determined from the simultaneous Monte Carlo analysis described above. The present uncertainty analysis does not yet include contributions from the systematics within the actual Coulomb dissociation measurement, as such an analysis requires numerous repeated simulations of the setup response, which have yet to be completed. Preliminary studies of systematic error in previous experiments performed with the R^3B-LAND setup have shown uncertainties in the yield on the order of 12%–15%. It should also be noted that while the present MACS determination relies on the choice of γ-ray strength function model used in the fit, the variation in the final capture rate was only 5% between two most commonly adopted formalisms [32,33] at astrophysical energies. The results of the present determination of the MACS for $^{59}\mathrm{Fe}(n,\gamma)^{60}\mathrm{Fe}$ are shown in Table I for temperatures relevant to shell burning in massive stars. Within the present uncertainty, the values of the present work agree with NON-SMOKER [37] predictions currently used in massive star models. The analysis described above will be expanded upon in an upcoming full paper currently in preparation.

While the stellar cross sections determined from the present measurement deviate only marginally from the previous theoretical values, this work provides a first experimental confirmation that the rates currently used in massive stars are not highly erroneous. Further, the present work offers a realistic quantification of the dominant remaining sources of uncertainty in the $^{59}\mathrm{Fe}(n,\gamma)^{60}\mathrm{Fe}$ rate. While challenges remain within the stellar models, the present study is an important step forward in realizing fully the potential of the observational constraint offered to present predictions of ^{26}Al and ^{60}Fe nucleosynthesis by γ-ray astronomy.

TABLE I. Maxwellian averaged cross sections[a] for $^{59}\mathrm{Fe}(n,\gamma)^{60}\mathrm{Fe}$

kT [keV]	80	85	90	95	100
Present	13.3	12.7	12.2	11.8	11.4
Error lower	−3.1	−3.0	−2.9	−2.8	−2.8
Error upper	+2.0	+1.9	+1.8	+1.8	+1.7
Reference [37]	11.2	10.8	10.3	10.0	9.6

[a]Cross section units are in millibarns.

This work was supported in part by NSF Grants No. PHY0758100 and No. PHY1068192, the Joint Institute for Nuclear Astrophysics (NSF Grant No. PHY0822648), the Helmholtz International Center for FAIR, the Helmholtz Alliance Program EMMI, the GSI-TU Darmstadt Cooperation agreement, the BMBF under Contracts No. 05P12RDFN8, the Helmholtz-CAS Joint Research Group (HGJRG-108), and the Helmholtz Association via the Young Investigators Grant No. VH-NG-627.

*Present address: Cyclotron Institute, Texas A&M University, College Station, TX 77843, USA.
uberseder@tamu.edu
†Present address: National Superconducting Cyclotron Laboratory, Michigan State University, East Lansing, MI 48824, USA.

[1] W. A. Mahoney, J. C. Ling, A. S. Jacobson, and R. E. Lingenfelter, Astrophys. J. **262**, 742 (1982).
[2] W. Fowler, Rev. Mod. Phys. **56**, 149 (1984).
[3] N. Prantzos and R. Diehl, Phys. Rep. **267**, 1 (1996).
[4] J. Knödlseder, Astrophys. J. **510**, 915 (1999).
[5] R. Diehl and F. Timmes, Publ. Astron. Soc. Pac. **110**, 637 (1998).
[6] F. Timmes, S. Woosley, D. Hartmann, R. Hoffman, T. Weaver, and F. Matteucci, Astrophys. J. **449**, 204 (1995).
[7] W. Wang, M. Harris, R. Diehl, H. Halloin, B. Cordier, A. Strong, K. Kretschmer, J. Knödlseder, P. Jean, G. Lichti *et al.*, Astron. Astrophys. **469**, 1005 (2007).
[8] D. Smith, New Astron. Rev. **48**, 87 (2004).
[9] D. M. Smith, in *Proceedings of the 5th INTEGRAL Workshop on the INTEGRAL Universe (ESA SP-552)*, edited by V. Schönfelder, G. Lichti, and C. Winkler (ESA Publications, The Netherlands, 2004), p. 45.
[10] M. Limongi and A. Chieffi, Astrophys. J. **592**, 404 (2003).
[11] T. Rauscher, A. Heger, R. Hoffman, and S. Woosley, Astrophys. J. **576**, 323 (2002).
[12] N. Prantzos, Astron. Astrophys. **420**, 1033 (2004).
[13] M. Limongi and A. Chieffi, Astrophys. J. **647**, 483 (2006).
[14] C. Tur, A. Heger, and S. Austin, Astrophys. J. **718**, 357 (2010).
[15] S. Woosley and A. Heger, Phys. Rep. **442**, 269 (2007).
[16] M. Limongi and A. Chieffi, New Astron. Rev. **50**, 474 (2006).
[17] E. Uberseder, R. Reifarth, D. Schumann, I. Dillmann, C. Domingo Pardo, J. Görres, M. Heil, F. Käppeler, J. Marganiec, J. Neuhausen *et al.*, Phys. Rev. Lett. **102**, 151101 (2009).
[18] C. Baglin, Nucl. Data Sheets **95**, 215 (2002).

[19] H. Geissel, P. Armbruster, K. Behr, A. Brünle, K. Burkard, M. Chen, H. Folger, B. Franczak, H. Keller, O. Klepper *et al.*, Nucl. Instrum. Methods Phys. Res., Sect. B **70**, 286 (1992).
[20] J. Cub, G. Stengel, A. Grünschloss, K. Boretzky, T. Aumann, W. Dostal, B. Eberlein, T. Elze, H. Emling, G. Ickert *et al.*, Nucl. Instrum. Methods Phys. Res., Sect. A **402**, 67 (1998).
[21] K. Boretzky, A. Grünschloß, S. Ilievski, P. Adrich, T. Aumann, C. A. Bertulani, J. Cub, W. Dostal, B. Eberlein, T. W. Elze *et al.* (LAND Collaboration), Phys. Rev. C **68**, 024317 (2003).
[22] T. Blaich, T. Elze, H. Emling, H. Freiesleben, K. Grimm, W. Henning, R. Holzmann, G. Ickert, J. Keller, H. Klinger *et al.*, Nucl. Instrum. Methods Phys. Res., Sect. A **314**, 136 (1992).
[23] V. Metag, D. Habs, K. Helmer, U. Helmolt, H. Heyng, B. Kolb, D. Pelte, D. Schwalm, W. Hennerici, H. Hennrich *et al.*, in *Detectors in Heavy-Ion Reactions*, edited by W. Oertzen, Lecture Notes in Physics Vol. 178 (Springer Berlin Heidelberg, 1983), pp. 163–178.
[24] C. Bertulani and G. Baur, Phys. Rep. **163**, 299 (1988).
[25] A. Koning and M. Duijvestijn, Nucl. Phys. **A744**, 15 (2004).
[26] T. Thomas, Nucl. Phys. **53**, 558 (1964).
[27] T. Thomas, Nucl. Phys. **53**, 577 (1964).
[28] D. Bertini, J. Phys. Conf. Ser. **331**, 032036 (2011).
[29] A. Junghans, G. Rusev, R. Schwengner, A. Wagner, and E. Grosse, Phys. Lett. B **670**, 200 (2008).
[30] P. Möller, J. Nix, W. Myers, and W. Swiatecki, At. Data Nucl. Data Tables **59**, 185 (1995).
[31] P. Axel, Phys. Rev. **126**, 671 (1962).
[32] C. M. McCullagh, M. L. Stelts, and R. E. Chrien, Phys. Rev. C **23**, 1394 (1981).
[33] J. Kopecky and M. Uhl, Phys. Rev. C **41**, 1941 (1990).
[34] A. Koning, S. Hilaire, and S. Goriely, *TALYS-1.4: A Nuclear Reaction Program* (Nuclear Research and Consultancy Group, Petten, The Netherlands, 2011), 1st ed.
[35] H. Utsunomiya, S. Goriely, H. Akimune, H. Harada, F. Kitatani, S. Goko, H. Toyokawa, K. Yamada, T. Kondo, O. Itoh *et al.*, Phys. Rev. C **82**, 064610 (2010).
[36] H. Utsunomiya, S. Goriely, H. Akimune, H. Harada, F. Kitatani, S. Goko, H. Toyokawa, K. Yamada, and Y.-W. Lui, J. Korean Phys. Soc. **59**, 1713 (2011).
[37] T. Rauscher and F.-K. Thielemann, At. Data Nucl. Data Tables **75**, 1 (2000).
[38] G. Michaud, L. Scherk, and E. Vogt, Phys. Rev. C **1**, 864 (1970).
[39] J. Holmes, S. Woosley, W. Fowler, and B. Zimmerman, At. Data Nucl. Data Tables **18**, 305 (1976).
[40] R. Capote, M. Herman, P. Oblozinsky, P. Young, S. Goriely, T. Belgya, A. Ignatyuk, A. Koning, S. Hilaire, V. Plujko *et al.*, Nucl. Data Sheets **110**, 3107 (2009).
[41] T. Rauscher, F.-K. Thielemann, and K.-L. Kratz, Phys. Rev. C **56**, 1613 (1997).
[42] H. Loens, K. Langanke, G. Martínez-Pinedo, and K. Sieja, Eur. Phys. J. A **48**, 34 (2012).
[43] B. Allen and R. Macklin, J. Phys. G **6**, 381 (1980).
[44] F. Käppeler, K. Wisshak, and L. Hong, Nucl. Sci. Eng. **84**, 234 (1983).